JOURNAL OF MATERIALS SCIENCE **39** (2004) 85–97

Magnetic measurements of martensitic transformation in austenitic stainless steel after room temperature rolling

K. MUMTAZ, S. TAKAHASHI, J. ECHIGOYA, Y. KAMADA, L. F. ZHANG, H. KIKUCHI, K. ARA, M. SATO
Non-Destructive Evaluation and Science Research Center, Faculty of Engineering, Iwate University, Morioka 020-8551, Japan
E-mail: fahadkm@hotmail.com

In order to investigate the detection of martensite phase in deformed austenitic stainless steel, magnetic properties were examined by means of super conducting quantum interface device (SQUID) and vibrating sample magnetometer (VSM) techniques. Stainless steel specimens were rolled at room temperature with 15 to 55% reduction in thickness. Results indicate that the magnetic properties of stainless steel were sensitive to percent reduction in thickness and micro structural condition of stainless steel. It was found that saturation magnetization, amount of martensite and hardness increased whereas, coercive force and remanence ratio decreased with increasing percent reduction in thickness. The saturation magnetization depends mainly on amount of martensite, while the coercive force and remanence depends mostly on shape and distribution of martensite phase.
© *2004 Kluwer Academic Publishers*

1. Introduction

The transformation from austenite to martensite is the principal phase transformation in stainless steel, and it has been the subject of numerous studies over the years, as it provides the basis for one of the most important structural materials [1–15]. Thus, an investigation into the martensitic transformation is of vital importance for practical structural design and the reliable utilization of the stainless steels.

The stainless steels are susceptible to martensitic transformation by plastic deformation, subzero cooling, subzero deformation, hydrogen charging, ion implantation and magnetron sputtering [1–22].

In stainless steels, the dislocations and twins are considered to be the major cause of martensitic phase transformation that is formed upon undergoing a plastic deformation or subzero treatments. The dislocations, twins, grain boundaries and grain size hold the key to the secular degradation or metallurgical stability of stainless steels, and the ability to detect these features is of great importance in safe operation of structural materials, such as turbine blades, nuclear reactors, bridges, and other large structures. There may be many other practical situations where this also becomes important, for example, in power plants where steel pipes are covered with thermal insulation.

The majority of conventional austenitic stainless steels (304, 304L, 316, 316L, etc.) are paramagnetic if they have an austenitic microstructure. However, these steels may become ferromagnetic when the bcc α' martensite state ($a = 2.86$ Å) is produced by plastic deformation. Therefore, it is possible to examine the properties of austenitic stainless steel in two distinct crystalline states.

Magnetic measurement techniques for non-destructive testing (NDT), inspection, and detection of gross defects such as surface and sub-surface cracks are well established [23–28].

There is current interest in the use of measurements of magnetic properties as a non-destructive evaluation (NDE) tool for monitoring and determining deformation and damage prior to crack initiation in stainless steels [29, 30]. This phenomenon may also be useful in investigating the mechanism of martensitic transformation, because magnetic measurement is more sensitive in this case than any other kind of measurements and may furnish various kinds of information about the mechanism of the transformation.

We selected Type 304 austenitic stainless steel for this study because of its obvious practical importance and because of the microstructural phenomena that occur during plastic deformation. In this work martensitic phase was introduced in austenitic stainless steel by rolling at room temperature to study the influence of martensitic transformation on magnetic properties.

2. Experimental procedure

The material used for the investigation was Type 304 austenitic stainless steel. The stainless steel was delivered as 100 mm length × 50 mm width × 1.85 mm

TABLE I Chemical composition of SUS 304 austenitic stainless steel

Element	C	Cr	Ni	Mn	Si	P	S	Fe
Content wt%	0.06	18.44	8.33	1.16	0.43	0.033	0.009	Bal.

thick hot-rolled plate stock. The chemical composition of the stainless steel is shown in Table I. The typical microstructure of the as-received stainless steel specimen is presented in Fig. 1. The grains size was determined as 25 μm. The grain structure was fully austenitic, containing a negligible volume percent of martensite as detected by magnetic measurement.

Specimens for room temperature rolling were prepared from the rolled plate parallel to the rolling direction by Spark wire cut machine (Fine Sodick Wire Cut EDM). For room temperature rolling, rectangular strips of size 100 mm length $\times$ 12 mm width $\times$ 1.85 mm thickness were used. The stainless steel specimens were subjected to room temperature rolling to achieve 15, 20, 25, 30, 35, 40, 45 and 55% reductions in thickness. The plastic strain rates were assumed to be essentially constant in all the cases. The temperature of the specimens also remains constant. At least three specimens were rolled at room temperature for different measurements.

After rolling, the stainless steel specimens of different reduction in thickness were cut into size of 3.5 mm $\times$ 3 mm in the rolling direction. All specimens were electro-polished using a 170 ml:30 ml solution of ethanol and perchloric acid at 30 V for 45 s prior to magnetic and hardness measurements.

The specimens were subsequently used for magnetic measurements, X-ray diffraction, hardness testing, scanning electron microscopy (SEM) and transmission electron microscopy (TEM).

X-ray diffraction (XRD) was carried out on the specimens to determine the crystallographic features and amount of martensite using a Material Analysis & Characterization M21X X-ray diffractometer with Cu K_α radiation. The degree of martensite formation was quantified by comparison of the integrated intensity ratios of the α' and γ reflections.

The saturation magnetization values were obtained from magnetization curves using a superconducting quantum interference device (SQUID) Design MPMS XL magnetometer at room temperature in an applied field of 0 to 30 kOe. The values of coercive force and remanence ratio were obtained from magnetic hysteresis loops with a vibrating sample magnetometer (VSM) at room temperature in an applied magnetic field of -20 to $+20$ kOe. Micro-hardness testing was done using Akashi MVK-FII hardness tester on the specimens with a mirror like surface finish obtained by electro-polishing.

The microstructures were characterized using JEOL JSM-5510 electron microscope (SEM). For SEM examination a mixture of nitric acid and hydrochloric acid (1:3) solution was used to etch the specimens. The microstructures were also characterized using transmission electron microscopy (TEM). TEM imaging was carried out with a Philips Technai-30 instrument with a double tilt holder operating at 200 kV. The TEM specimens were prepared parallel to the surface (planar section) of the specimens. Thin foils were prepared by polishing roughly to 80 μm. Subsequent thinning was carried out by twin jet electro-polishing in solution of

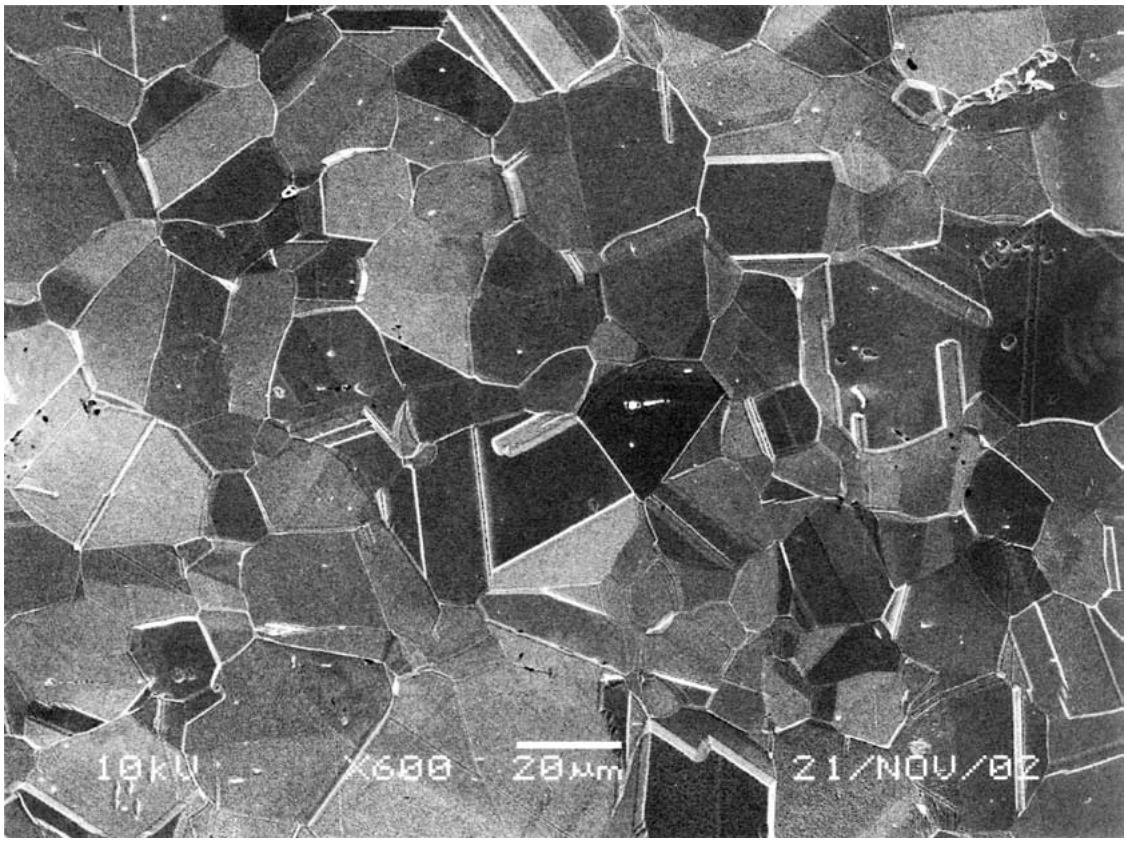

Figure 1 SEM micrograph of as-received austenitic stainless steel.

perchloric acid and acetic acid (volume ratio was 1:9) at the voltage of 40–45 V.

3. Results

3.1. Scanning electron microscopy

Fig. 2a to c show the scanning electron micrographs of the austenitic stainless steel specimens with 20, 40, and 55% reduction in thickness, respectively. Comparing the grain size of the specimens that is rolled to 20% reduction to that of 55% reduction, there is significant difference in the grain size and grains are elongated in the rolling direction. Observations on a number of grains confirmed that there are more streaks and fault bands formed on the specimens with 40 and 55% reduction than 20% reduction in thickness. At the smaller percent of reduction in thickness the fault bands and streaks are much less in number [31]. No such streaks and fault bands are observed in the as received specimen (Fig. 1). The diffuse nature of grains in the specimens with 40 and 55% reduction is apparently a manifestation of severe distortion.

3.2. Magnetization

Ferromagnetic phase is introduced in stainless steel by room temperature rolling and is quantified by magnetization measurement. Fig. 3 shows the magnetization plotted as a function of the magnetic field for the as-received and 15 to 55% reduction in thickness specimens. There exists negligibly small magnetization in the as-received specimen. As seen from Fig. 3, compared to the as-received specimen, 15 to 55% reduction increases the magnetization of the specimens. It is found that the magnetization increases with the progress in rolling and maximum magnetization is obtained in the specimen with 55% reduction. Fig. 3 also shows that there is little difference between the magnetization values of the specimens after 15 and 20% reduction in thickness.

3.3. Hysteresis loops

The magnetic properties of a material are usually characterized by a hysteresis loop, which gives the behavior of a material when excited by an external magnetic field. Hysteresis loops of the specimens after 15 and 55% reduction in thickness are shown in Fig. 4a and b, respectively. The hysteresis loops are different for the specimens with 15 and 55% reduction in thickness. For example, a width of the hysteresis loop for the specimen with 15% reduction is larger than that for the specimen with 55% reduction. The width of the hysteresis loop became narrower with the increase of percentage reduction in thickness. The coercive force and remanence ratio decreases when the specimen underwent progress in rolling.

3.4. Saturation magnetization & coercive force

The saturation magnetization values are obtained from magnetization curves. Fig. 5 shows maximum

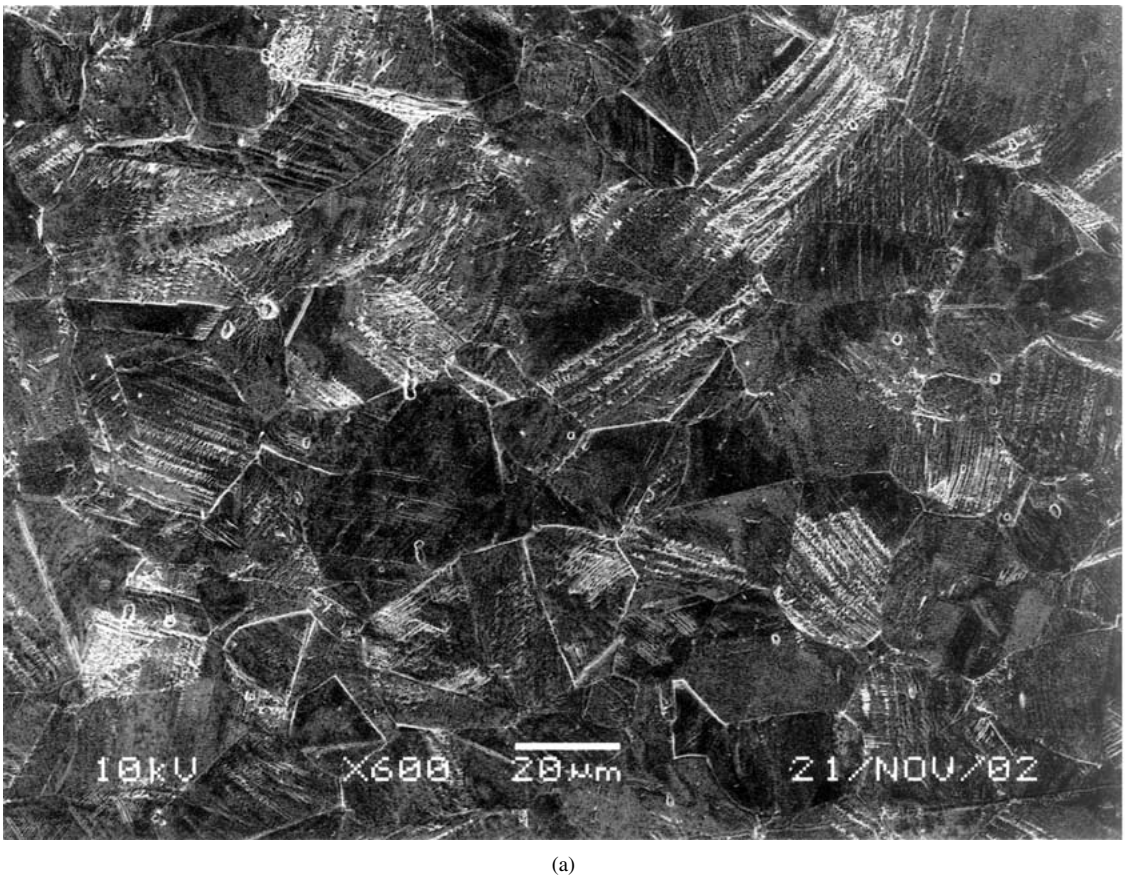

(a)

Figure 2 SEM micrographs of austenitic stainless steel specimens after rolling: (a) 20% reduction, (b) 40% reduction, and (c) 55% reduction in thickness. (*Continued*)

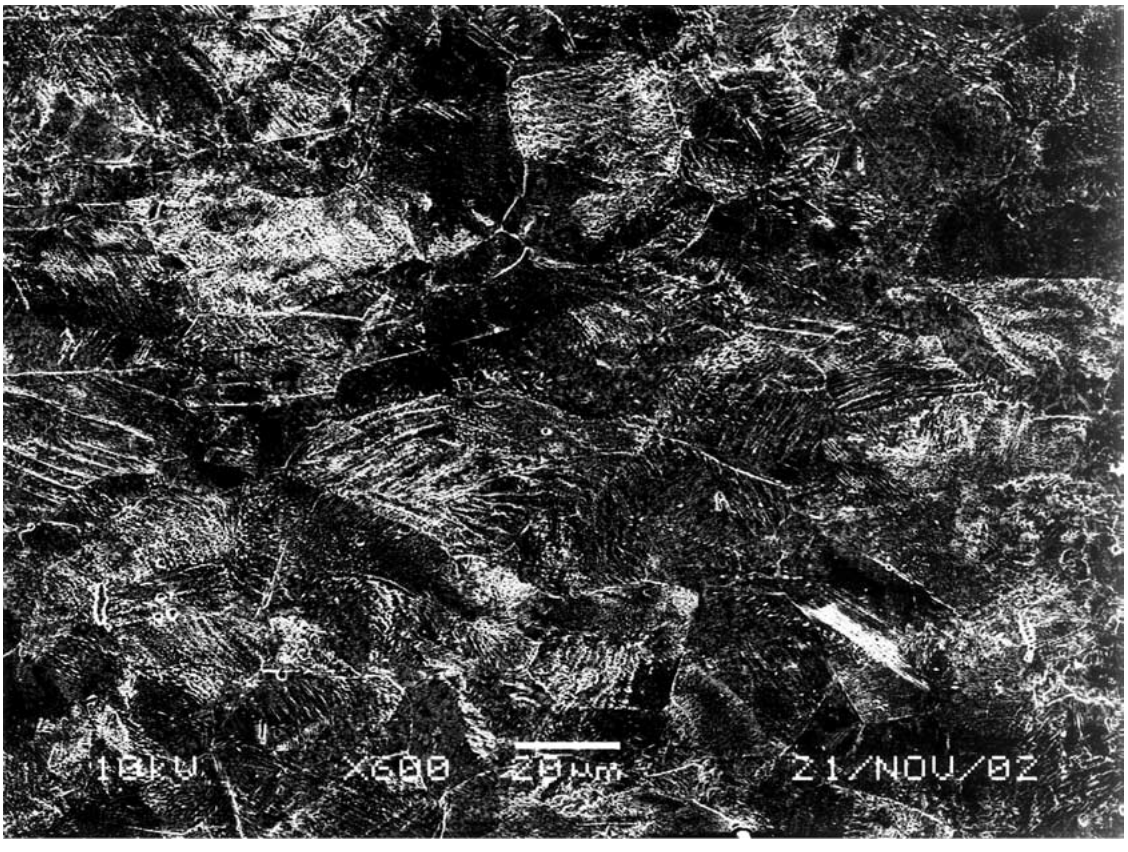

(b)

(c)

Figure 2 (*Continued*).

saturation magnetization and coercive force as a function of percentage reduction in thickness.

The saturation magnetization, which is in proportional to the volume percent of the ferromagnetic phase, is obtained from extrapolating the linear parts of magnetization curves back to the zero applied field. In this study, only α' martensite is ferromagnetic. The value of the saturation magnetization 154 emu/g, corresponds to

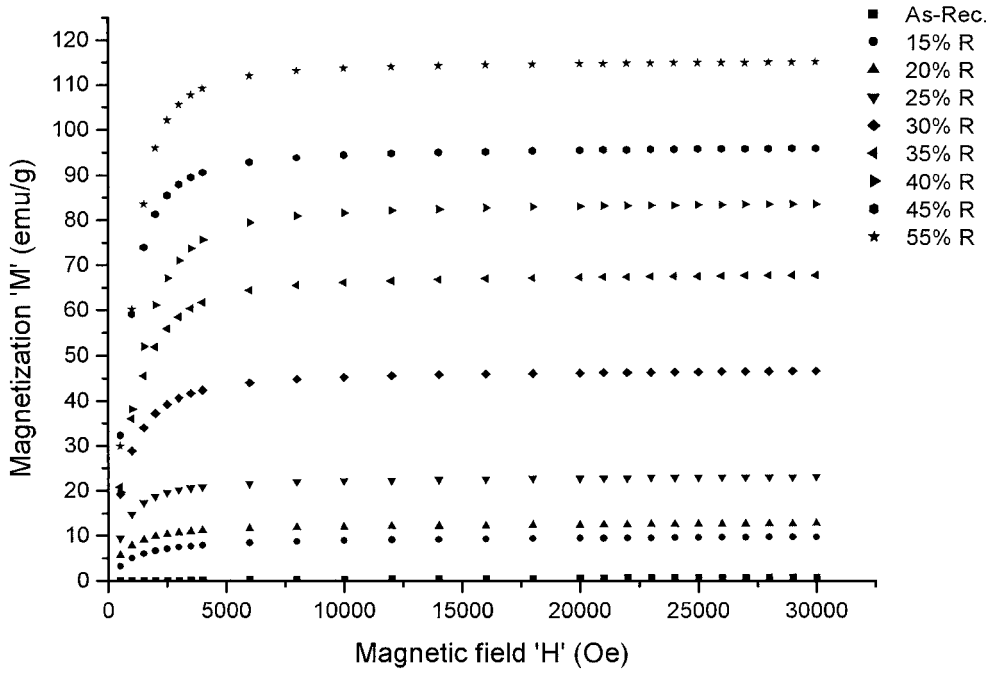

Figure 3 Magnetization plotted against magnetic field for as-received and after 15 to 55% reduction in thickness specimens.

the 100% α' martensite phase [32]. The value of the saturation magnetization in the as-received specimen was about 0.03 emu/g, which shows 2×10^{-2}% ferromagnetic phase in volume was included in the specimen. The saturation magnetization shows a remarkable increase with increasing percent reduction in thickness. The value of saturation magnetization after 55% reduction at room temperature was 113.92 emu/g, corresponding to about 74 volume percent of ferromagnetic phase.

Table II shows the magnetic properties, volume percent of α' martensite and hardness values of the as received and 15 to 55% reduction in thickness specimens.

Fig. 5 also shows the coercive force measurement result in the austenitic stainless steel specimens after 15 to 55% reduction at room temperature. The coercive force varied with percentage reduction in thickness in just the opposite way from the saturation magnetization. Coercive force is found to decrease with the increase in percent reduction and depends on the shape, distribution and volume percent α' of martensite phase. At 0% reduction, the specimen with austenitic phase has a coercive force 32.21 Oe in X direction (Table II). As shown in Fig. 5, the specimen with 15% reduction has a high value of coercive force (166.6 Oe), followed by a sharp decrease in coercive force with the increase in percent reduction in thickness. The specimen with 55% reduction has the lowest coercive force, about 48.71 Oe, and hence, the highest saturation magnetization. This result also shows that with 45 to 55% reduction there is not much difference in the value of the coercive force.

The magnetic measurements were also performed in three directions for each specimen: parallel to the rolling direction (X), perpendicular to the rolling direction (Y), and perpendicular to X and Y direction (Z), as shown in Fig. 6. The coercive force depends on the magnetization direction and the results are shown in Table II. The coercive force in Z direction that ranges from 234.9 Oe to 74.08 Oe for 15 and 55% reduction, respectively, and the values are higher as compared to the values in X and Y directions. The coercive force decreases with the increase of percentage reduction in all three directions. Results also show that in the X and Y directions with the increase in percent reduction the difference in coercive force decreases, and for 55% reduction the values of the coercive force are nearly same.

TABLE II Magnetic properties, volume percent of α' martensite, γ austenite and hardness values of the as received and rolled specimens

S. no.	Red. (%)	M_s (emu/g)	α' (%)	γ (%)	Rem. ratio	H_c(Oe) (X)	H_c(Oe) (Y)	H_c(Oe) (Z)	Hardness HV
CR-0	0	0.03	0.02	99.98	0.005	32.21	32.59	40	193
CR-1	15	8.78	5.70	94.30	0.22	166.6	189.7	234.9	296
CR-2	20	11.81	7.67	92.33	0.18	137.6	155.7	204.0	325
CR-3	25	22.08	14.34	85.66	0.14	108.2	126.1	180.0	355
CR-4	30	45.29	29.41	70.59	0.09	79.65	94.28	145.2	383
CR-5	35	66.33	43.07	56.93	0.06	65.02	75.34	120.7	407
CR-6	40	82.02	53.26	46.74	0.04	57.00	63.66	100.0	427
CR-7	45	94.58	61.41	38.59	0.04	48.83	52.47	82.07	475
CR-8	55	113.92	73.97	26.03	0.03	48.71	49.51	74.08	485

M_s: saturation magnetization, H_c: coercive force, rem. ratio: remanence ratio.

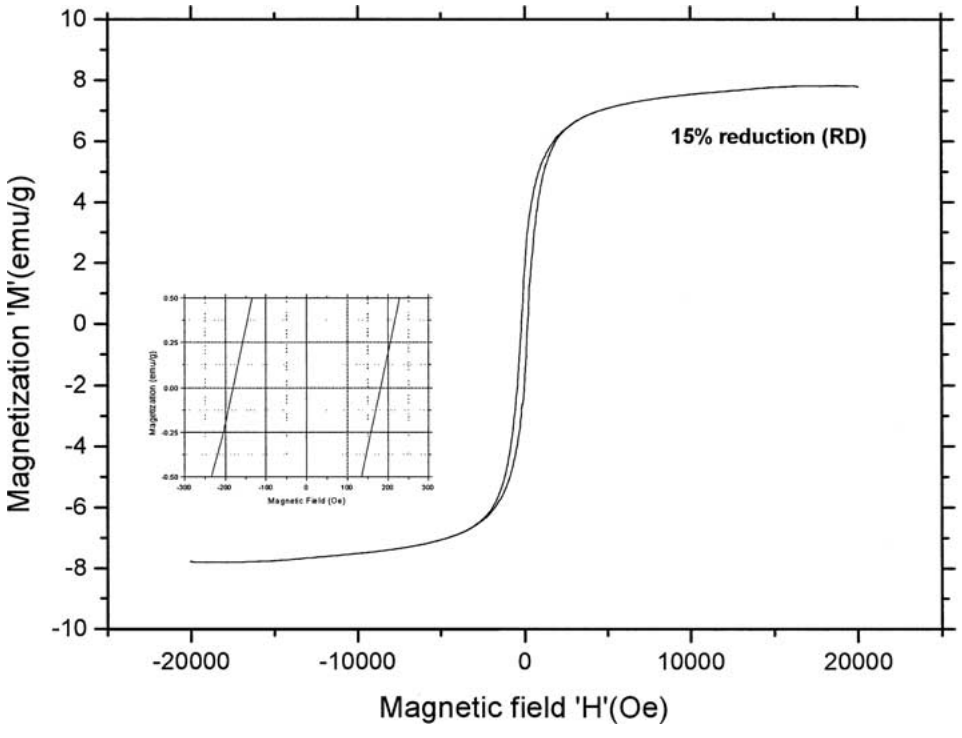

(a)

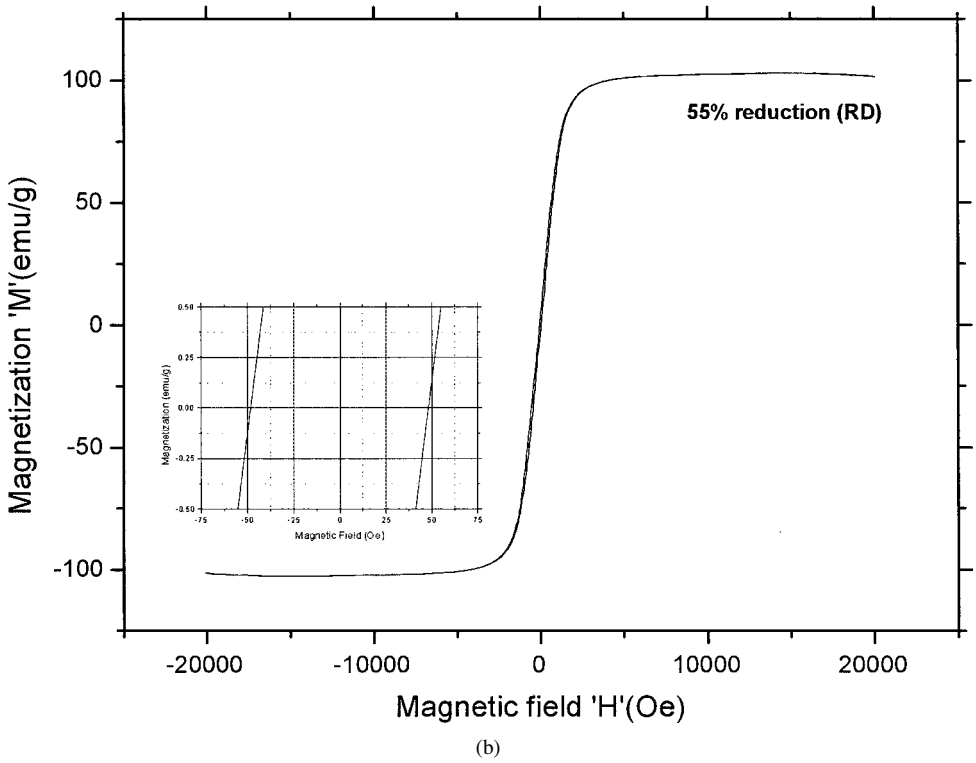

(b)

Figure 4 Hysteresis loops for stainless steel after: (a) 15% reduction and (b) 55% reduction in thickness.

3.5. Remanence ratio (M_r/M_s ratio)

Fig. 7 shows the remanence ratio and coercive force measured as a function of percent reduction in thickness. The remanence ratio decreases with progress in rolling, the specimen with 15% reduction remanence ratio is measured to be 0.22 and for 55% reduction it is 0.03. This indicates that the magnetic properties of stainless steels are related to the volume percent of α' martensite and its shape. The remanence ratio also showed the same behavior as the coercive force.

3.6. Volume percent of α' martensite and γ austenite

The volume percent of α' martensitic transformation, which is calculated from the value of saturation magnetization, primarily depends on the percent reduction in thickness. The volume percent of α' martensite and γ austenite plotted against percent reduction in thickness are shown in Fig. 8.

The magnetic measurement shows that with the progress in rolling, the volume percent of α' martensite increases and γ austenite decreases. The magnetic

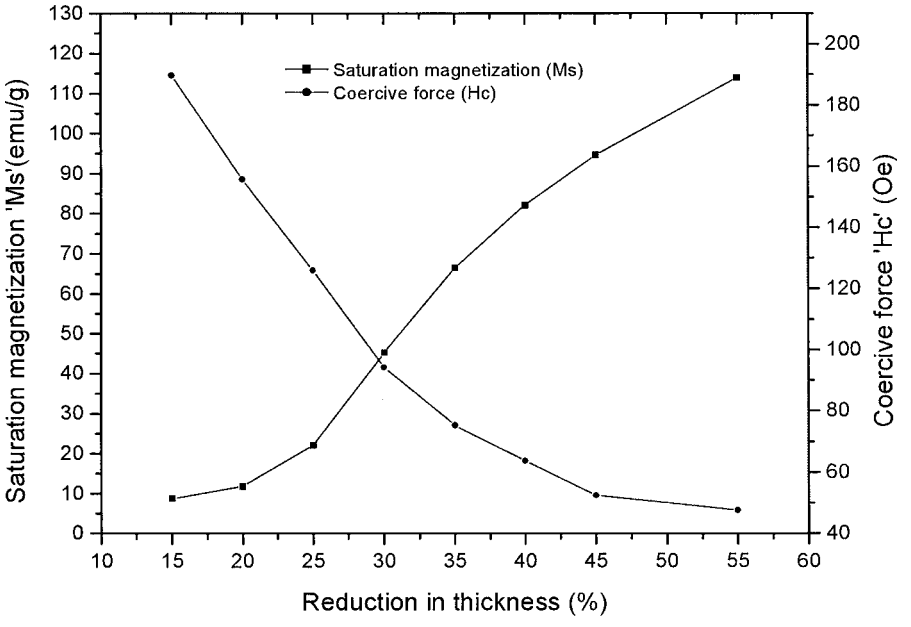

Figure 5 Saturation magnetization and coercive force plotted against percent reduction in thickness.

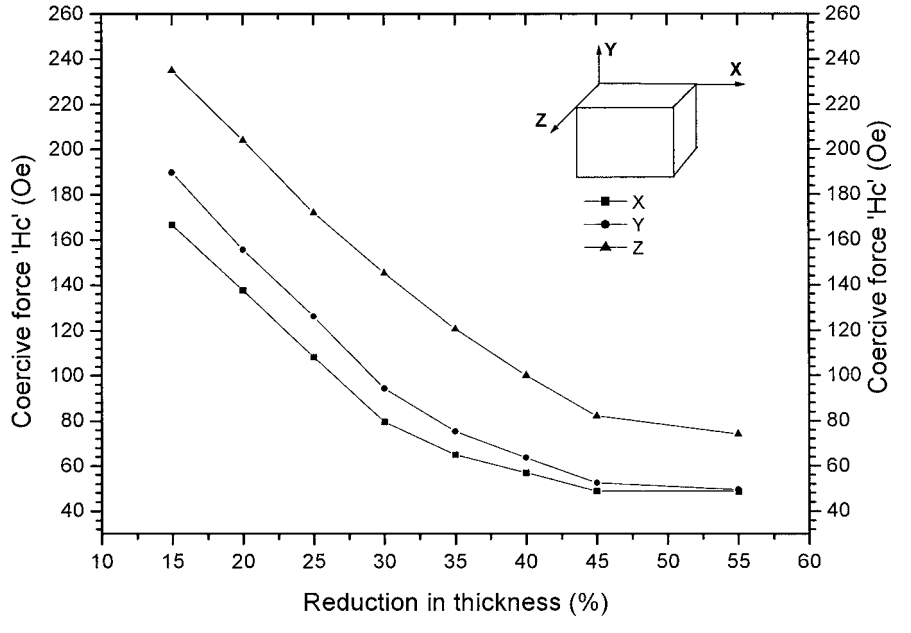

Figure 6 Coercive force plotted against percent reduction in thickness. (X) parallel to rolling direction, (Y) perpendicular to rolling direction and (Z) perpendicular to (X) and (Y).

transition indicates that 5.7 volume percent of α' martensitic phase is formed in the specimen with 15% reduction. The results also show that with 55% reduction the maximum value of α' martensitic phase about 74 percent volume is induced in the specimen. The martensite is a parasitic ferromagnetism and has a saturation magnetization of 62 emu/g in the plastically deformed specimen at 25°C [21]. This leads to the conclusion that the magnetization in the rolled specimens originates from α' martensite transformation. The large increase in the α' martensite transformation occurred above 20% reduction in thickness.

The volume percentage of γ decreases with the increase of percent reduction in thickness, whereas the volume percentage of α' martensite increased steadily with progress in rolling.

3.7. X-ray diffraction

X-ray diffraction was also used to determine the relative amounts of different phases formed in the austenitic stainless steel after rolling. The volume percent of α' martensite phase was calculated from the integrated intensity ratios of γ austenite and α' martensite peaks. Fig. 9 compares the X-ray diffraction patterns of the as-received specimen with reference to specimens after 40 and 55% reduction in thickness. X-ray diffraction data at room temperature showed that as-received stainless steel was single phase fcc (γ) with lattice parameter $a = 3.60$ Å. The ratio of the two phases depends on the percent reduction in thickness and the rolled specimens consisted of a mixture of two phases, bcc (α') with $a = 2.88$ Å and fcc (γ) with $a = 3.60$ Å. Table III summarises all the phases detected and the calculated

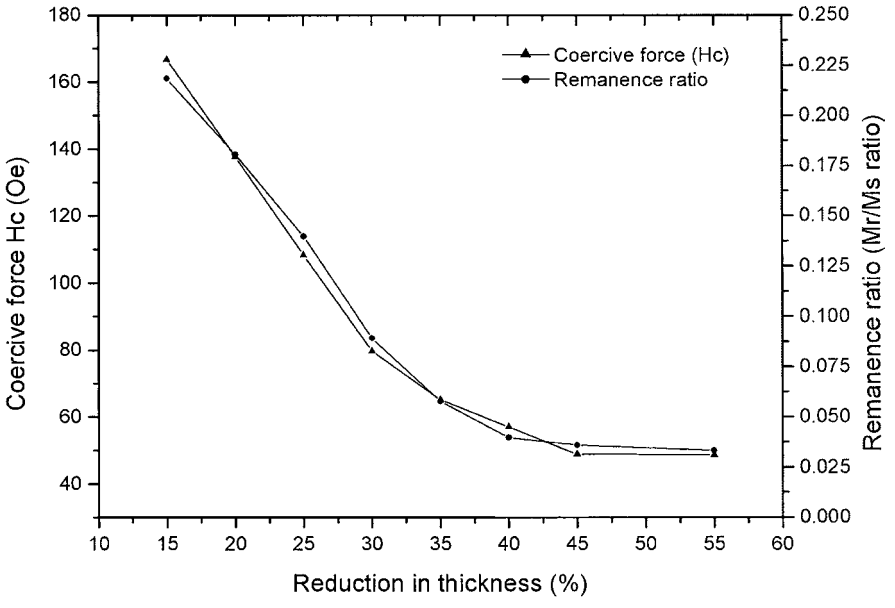

Figure 7 Remanence ratio and coercive force plotted against percent reduction in thickness.

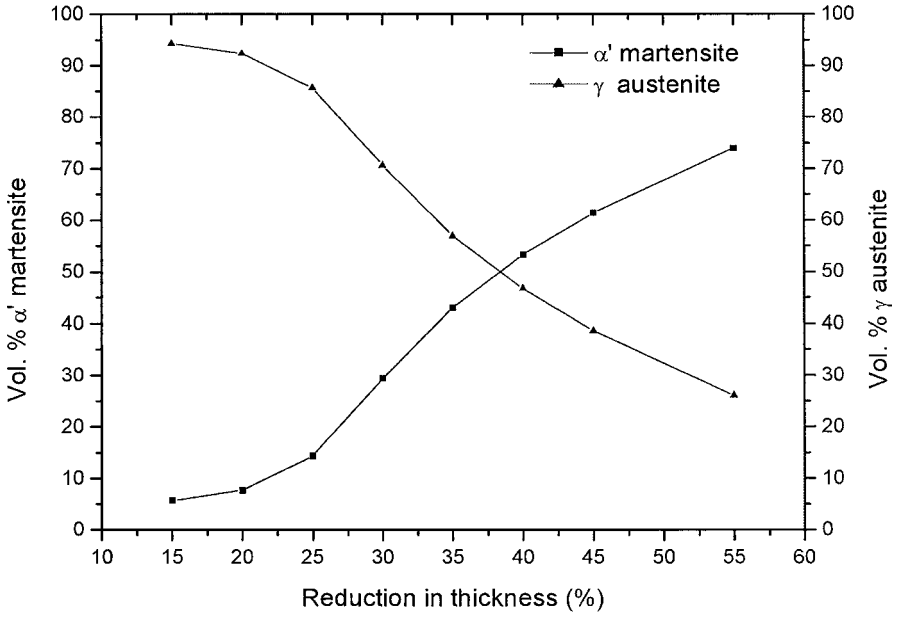

Figure 8 Volume % of α' martensite and γ austenite plotted against percent reduction in thickness.

amount of α' martensite in as-received and after 40 and 55% reduction in thickness specimens. It can be seen that the X-ray diffraction patterns for both as-received and rolled specimens exhibit all γ austenitic peaks, but in the case of specimens with 40 and 55% reduction, α' martensite peaks are also observed indicating that α' martensite phase was generated in the specimens in the process of rolling. The 55% reduction causes a prominent increase in peak intensity of α' martensite at a diffraction angle of $2\theta = 44.32$. The 40% rolling reduction also causes an increase in the intensity of the α' martensite peak in the, (200) and (211) planes. The intensity of α' martensite peak decreases with decreasing percent reduction in thickness. In the X-ray diffraction patterns, α' martensite phase is seen to be present in traces but they were hardly discernable after 15% reduction figure not shown. Therefore, the quantification of α' martensite by X-ray diffraction was very difficult below 20% reduction in thickness. Intensity measurement also shows that the relative volume percent of α' martensite reached a maximum amount after 55% rolling reduction, and the volume percent of α' martensite decreased steadily with decreasing level of percent reduction. The X-ray

TABLE III Phase detection and volume percent of α' martensite by XRD of as received and rolled specimens of austenitic stainless steel

Specimen no.	Volume % α' martensite	Phases
CR-0%	–	γ (111), γ (200), γ (220), γ (311),
CR-55%	64.58	γ (111), γ (200), γ (220), γ (311), α' (110), α' (200), α' (211)
CR-40%	43.52	γ (111), γ (200), γ (220), γ (311), α' (110), α' (200), α' (211)

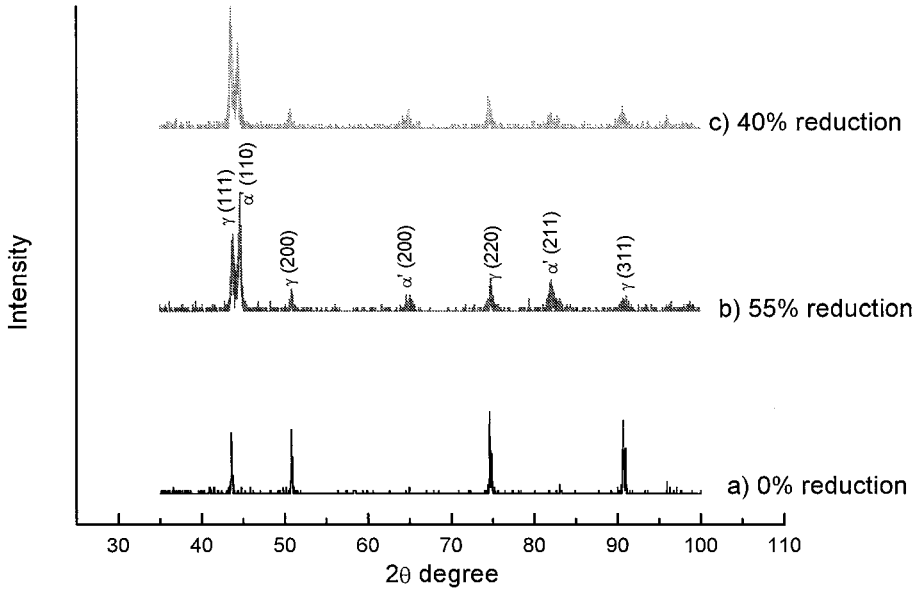

Figure 9 X-ray diffraction patterns of austenitic stainless steel: (a) as-received, (b) 55% reduction, and (c) 40% reduction.

diffraction patterns show no existence of any other phase.

3.8. Hardness

Fig. 10 shows the coercive force and hardness values plotted against percent reduction in thickness. The hardness increased with an increase in percent reduction, and after a 55% reduction in thickness, a hardness value of 485 HV is obtained. The hardness value of the as-received specimen was about 193 HV. Coercive force also reveals a simple dependence on hardness, and it decreased with the increase in hardness, as shown in Fig. 10. The coercive force and hardness value show the same trend after 45 and 55% reduction and their respective values are nearly the same. The high hardness value is associated with the transformation of austenite to α' martensite.

3.9. Transmission electron microscopy

Fig. 11a to c show bright-field micrographs and corresponding diffraction patterns for specimens deformed with 20, 40 and 55% reduction in thickness, respectively. After 20% reduction in thickness, α' martensite appeared only in a few grains, apparently because of low plastic strain. Magnetic measurement shows that 5.7 volume percent of α' martensite was formed in this specimen. The α' martensite was nucleated at intersections of shear bands as shown in Fig. 11a. The areas of dark phase are austenite regions while the light regions are α' martensite (indicated by arrows). The microstructure also has a considerable number of dislocations. The selected area diffraction pattern appears to be a double pattern, one set of diffraction spots corresponding to γ austenite (fcc) crystals, the other set corresponding to α' martensite (bcc) crystals. With an increase in percent reduction, the amount of α' martensite became greater,

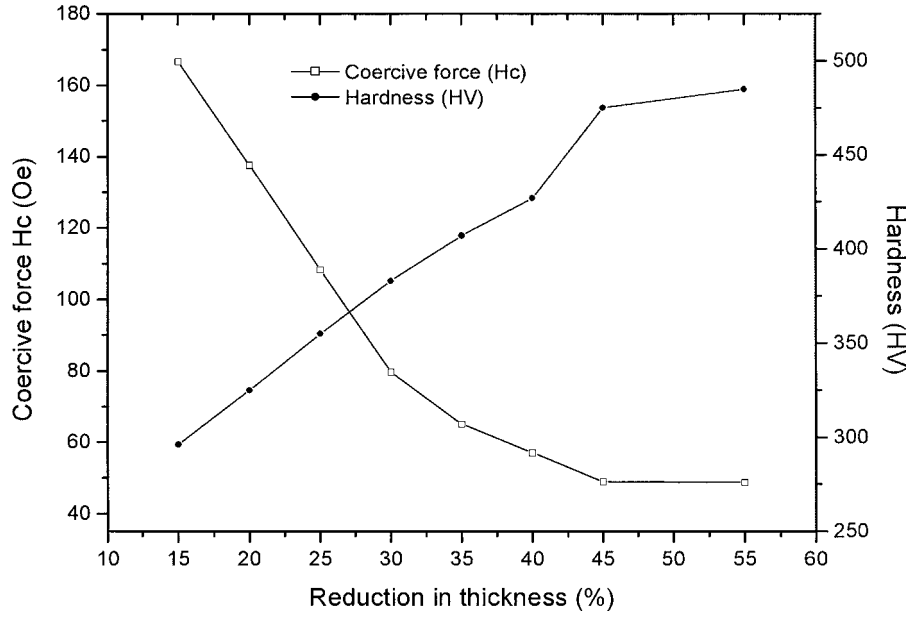

Figure 10 Coercive force and hardness plotted against percent reduction in thickness.

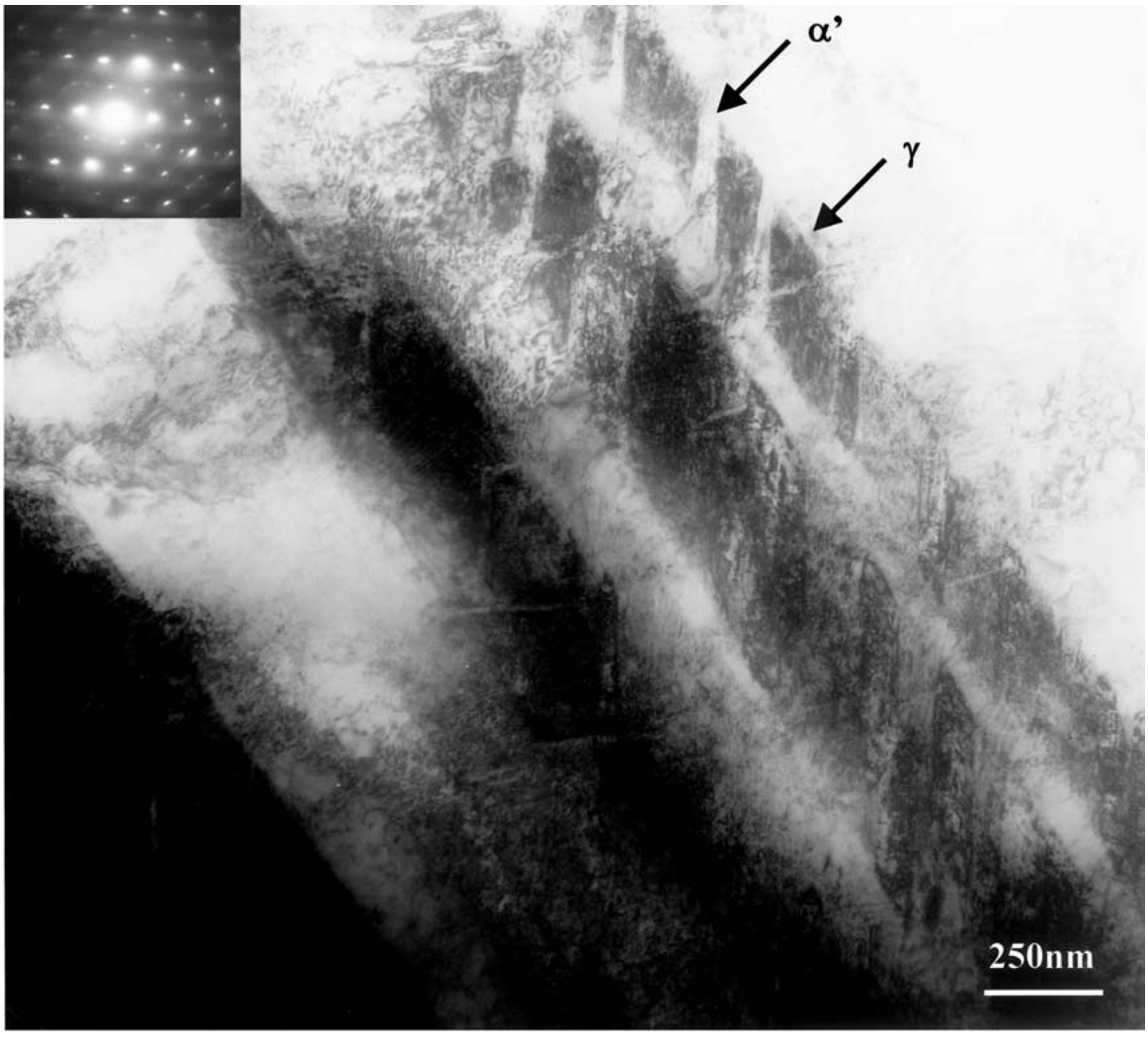

(a)

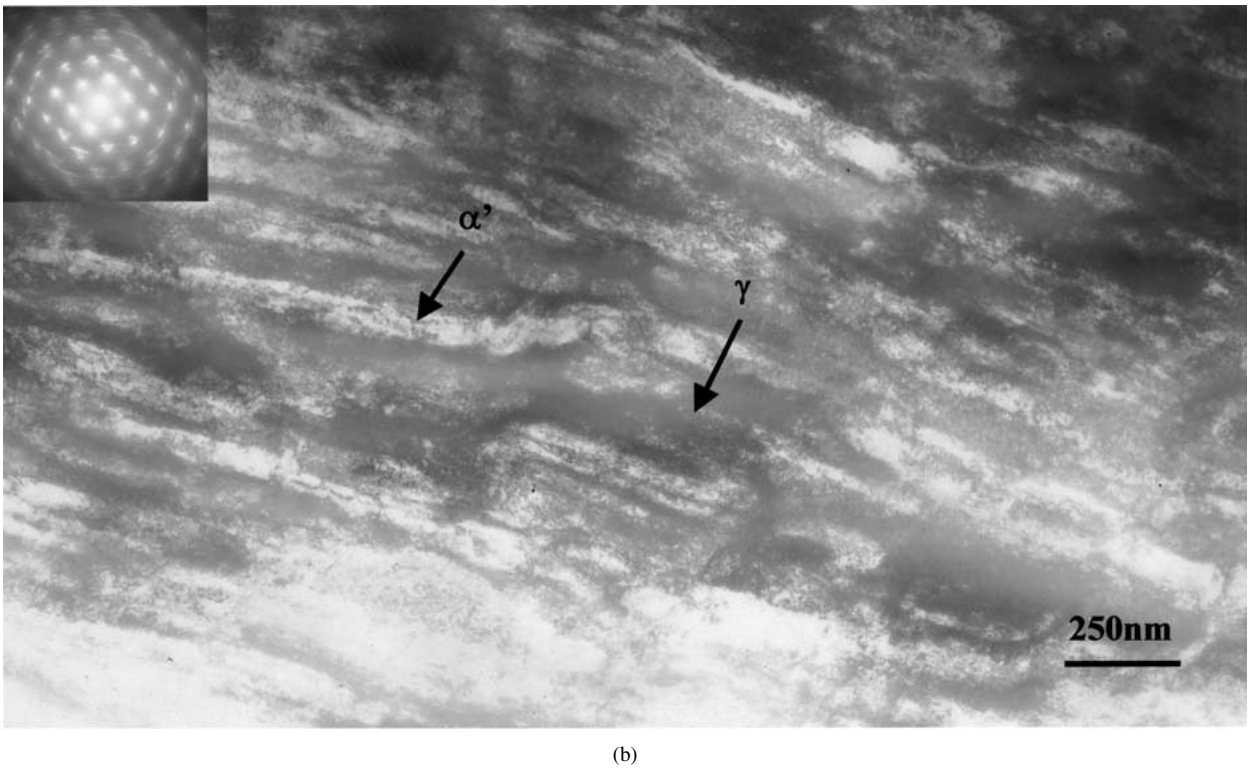

(b)

Figure 11 TEM micrographs and selected area diffraction patterns of austenitic stainless steel specimens after: (a) 20% reduction, (b) 40% reduction, and (c) 55% reduction in thickness. (*Continued*)

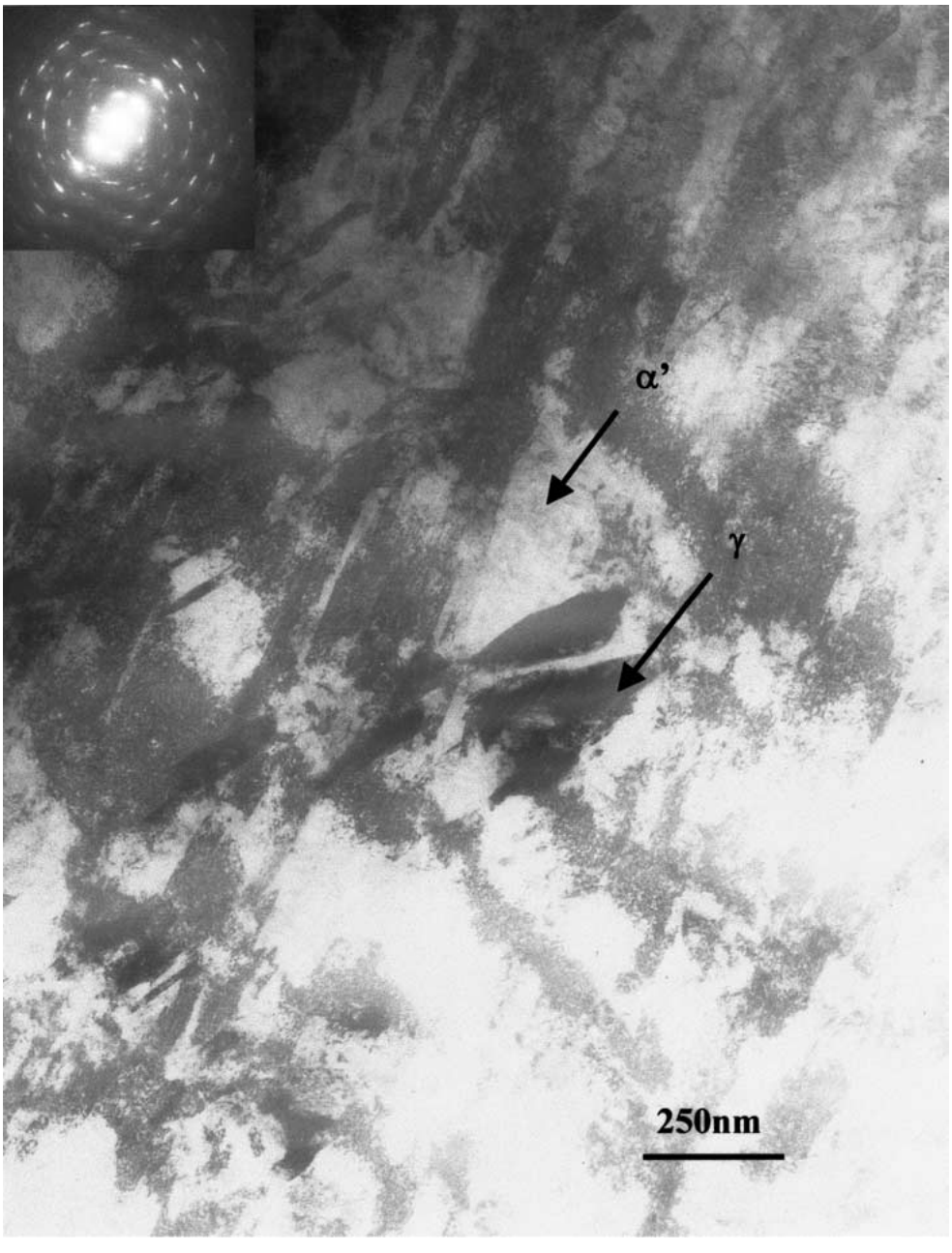

(c)

Figure 11 (*Continued*).

and it occurred in more grains. With progress in rolling, the density of these defects increases. After 40% reduction, evidence of α' martensite lath and bundles of faults intermixed with deformation twins develop. The bright-field image of a continuous long lath of α' martensite is shown in Fig. 11b. Magnetic measurement indicated that 53% of α' martensite is formed in this specimen. In stainless steel specimens after 55% reduction, α' martensite takes on an irregular blocky shape with an increase in dislocation density, as shown in Fig. 11c. The selected area diffraction pattern shows no trace of reflections from ε martensite in any specimens.

4. Discussion

The austenitic stainless steel rolled with different percent reduction in thickness has coexisting phases of austenite and martensite, which differ from each other structurally, and which therefore also differ in their intrinsic magnetic properties. Since the phases coexist microscopically and since only martensite phase has ferromagnetism, it can be supposed that magnetic properties are determined from the volume of ferromagnetic phase. In particular, magnetization, saturation magnetization, hysteresis loops, coercive force, and remanence ratio vary with volume percent of α' martensite. Usually, annealed austenitic stainless steels are paramagnetic at room temperature. Saturation magnetization should be zero. Saturation magnetization and transformation of α' martensite are found to be dependent on the percent reduction in thickness. The phenomenon of the saturation magnetization of stainless steel with progress in rolling is interpreted as follows: embryos of α' martensite are created by rolling and grow to some definite volume in the shape of laths, which is determined by the number of mobile dislocations produced

by that percent reduction in thickness. Since dislocations become harder to move with greater reduction in rolling, laths begin to grow in the form of irregular blocks. Therefore, formation of the ferromagnetic phase in a paramagnetic matrix is accompanied by an increase in saturation magnetization. This is in agreement with the result of TEM observations, which show that for small and medium percent reduction in thickness, transformed α' martensite is found to be lath like, whereas after 55% reduction, irregular blocky shape structures of α' martensite are formed (Fig. 11). Results show that saturation magnetization depends only on the quantity of the ferromagnetic phase. Therefore, NDE techniques can be exploited to enhance the saturation magnetization as a technique for detecting subsurface changes in deformed stainless steel.

The coercive force varied with percent reduction in thickness in just the opposite way from the saturation magnetization (Fig. 5). The coercive force behaves in an opposite manner in stainless steel as compared to ferromagnetic materials, and it decreases with the progress in rolling. The average size, shape, and distribution of martensitic phase determine the magnetic behavior of the stainless steel. The observation of hysteresis loops shows that they are sensitive to the percent reduction in thickness and hysteresis width is changed with the volume percent of α' martensite. Progress in rolling enables the coalescence of the martensite phase. After 55% reduction in thickness, more stable long and broad martensite is formed (Fig. 11c). The α' martensite phase has a strong magnetic anisotropy and coercive force is large, when its volume is small. Therefore, the decrease in coercive force may be associated with the shape of the martensite, and the magnetic anisotropy may be decreased when blocky martensite is formed. Furthermore, with the increase in martensite the pinning length of domain wall may be increased which resulted in decrease of the coercive force.

The coercive force also depends on the measurement direction, as shown in Fig. 10. This also suggests that, shape of martensite phase and its distribution is affecting coercive force. The remanence ratio that is closely related to coercive force is shown in Fig. 7. The remanence ratio is also indicative of the degree of anisotropy in the material [33]. The two curves are similar, indicating the same mechanisms of shape magnetic anisotropy. The coercive force also revealed a simple dependence on hardness as shown in Fig. 10. After rolling, martensite phase and crystal defects such as dislocations are induced in the specimens. The strength of the stainless steel is determined by the production and motion of dislocations [34]. In a rolled stainless steel the increased strength is caused by the increase in martensitic phase. Generally, an increase in plastic deformation induced the increasing barrier for dislocation motion and the nucleation of martensite induces a high hardness. As the rolling progresses, new martensite laths were nucleated. The presence of slip pile-ups, streaks and bands in the grains are also observed Fig. 2c. The presence of pile-ups have the role of increasing the slip resistance [35], hence hardening the matrix, at the same time generating considerable internal stresses. The generation of more defects and the increase of local pile-up stresses lead to the observed increase in the hardness. Results show that coercive force may also be used as a measure of hardness of the stainless steel, which gives a useful nondestructive evaluation of an important mechanical property. The above results certainly provide some indication of the merits of the magnetization measurements.

5. Conclusions

The detection of α' martensite phase in austenitic stainless steel after 15 to 55% reduction in thickness was investigated and the following conclusions were obtained.

1. Saturation magnetization was increased with increasing percent reduction in thickness. The reason for this is the increasing volume percent of α' martensite.
2. Magnetic hysteresis curves change depending on the percent reduction in thickness and hence volume percent of α' martensite.
3. Coercive force and remanence ratio decreased with increasing percent reduction in thickness. These results were attributed to the shape magnetic anisotropy due to formation of different shape of martensite.
4. Hardness value was increased with an increasing percent reduction in thickness. This would be caused by martensite phase being formed in the austenitic matrix.
5. With a small percent reduction in thickness, martensite begins to form, and with the progress of rolling, long and narrow martensite laths nucleated and after high percent reduction in thickness become irregular blocky shape.

Acknowledgements

This work was partly supported by the Grant-in-Aid for Scientific Research on Priority Areas under Scientific Research (S) No. 14102034 from the Ministry of Education, Culture, Sports, Science and Technology, Japan.

References

1. C. B. POST and W. S. EBERLY, *Trans. Amer. Soc. Metals* **39** (1947) 868.
2. H. C. FIELDER, B. L. AVERBACH and M. COHEN, *Trans. Amer. Soc. Metals* **47** (1954) 267.
3. B. EDMONDSON and T. KO, *Acta Metall.* **2** (1954) 233.
4. P. G. BASTEIN and J. M. B. DEDIEU, *J. Iron Steel Inst.* **183** (1956) 254.
5. G. B. OLSEN and M. COHEN, *Metall. Trans.* A **7A** (1976), 1897.
6. *Idem.*, *ibid.* **7A** (1976), 1905.
7. G. B. OLSEN and M. AZRIN, *ibid.* **9A** (1978), 1897.
8. S. S. HECKER, M. G. STOUT, K. P. STAUDHAMMER and J. L. SMITH, *ibid.* **13A** (1982) 619.
9. C. J. GUNTER and R. P. REED, *Trans. ASM* **55** (1962) 399.
10. P. L. MANGONON, JR. and G. THOMAS, *Metall. Trans.* **1** (1970) 1577.
11. J. W. BROOKS, M. H. LORETTO and R. E. SMALLMAN, *Acta Metall.* **271** (1979) 829.
12. T. MAKI and C. M. WAYMAN, *ibid.* **25** (1977) 681.
13. H. WARLIMONT, *Metall. Trans.* **2** (1971) 1847.

14. P. M. KELLY and J. NUTTING, *J. Iron Steel Inst.* **184** (1961) 199.
15. R. LANGEBORG, *Acta Metall.* **12** (1964) 823.
16. T. SUZUKI, H. KOJIMA, K. SUZUKI, T. HASHIMOTO and M. ICHIHARA, *ibid.* **25** (1977) 1151.
17. R. P. REED, *ibid.* **10** (1962) 865.
18. V. SEETHARAMAN and R. KRISHNAN, *J. Mater. Sci.* **16** (1981) 523.
19. J. F. BREEDIS, *Acta Metall.* **13** (1965) 239.
20. S. D. DAHLGREN, *Metall. Trans.* **1** (1970) 3095.
21. J. CHILDRESS, S. H. LIOU and C. L. CHIEN, *J. de Phys.* **49** (1988) C8-118.
22. J. P. EYMERY and R. KRISHNAN, *J. Mag. Mag. Mater.* **104–107** (1992) 1785.
23. F. A. GARNER, F. ABE and T. NODA, *J. Nucl. Mater.* **155–157** (1992) 870.
24. N. HASHIMOTO, S. J. ZINKLE, A. F. ROWCLIFF, J. P. ROBERTSON and S. JITSUKAWA, *J. Nucl. Mater.* **283–287** (2000) 528.
25. P. KAUPPINEN and J. SILLAMPAA, *The Intern. J. Press. Vess. Pip.* **54** (1993) 523.
26. P. KAUPPINEN and P. SARKINIEMI, *ibid.* **55** (1993) 141.
27. J. R. BOWLER, Recent Advances and Challenges in Eddy Current Non-Destructive Evaluation Techniques, The 10th International Symposium on Applied Electromagnetic and Mechanics, May 13–16, 2001, Tokyo, Japan.
28. T. TANIGUCHI, K. NAKAMURA, D. KACPRZAK, S. YAMADA and M. IWAHARA, Eddy-Current Testing Image Processing for Extraction of Orientation of Defects The 10th International Symposium on Applied Electromagnetic and Mechanics, May 13–16, 2001, Tokyo, Japan.
29. S. TAKAHASHI, J. ECHIGOYA and Z. MOTOKI, *J. Appl. Phys.* **87**(2) (2000) 805.
30. S. TAKAHASHI, J. ECHIGOYA, T. UEDA, X. LI and H. HATAFUKU, *J. Mater. Proc. Techno.* **108** (2001) 213.
31. K. MUMTAZ, S. TAKAHASHI, J. ECHIGOYA, L. F. ZHANG, Y. KAMADA and M. SATO, *J. Mater. Sci. Lett.* **21** (2002) 1199.
32. M. B. STEARNS, *Phys. Rev.* **13** (1976) 1183.
33. R. M. BOZORTH, "Ferromagnetism" (IEEE Press, 1993).
34. J. D. VERHOVEN, "Fundamentals of Physical Metallurgy" (Wiley, New York, 1975) p. 405.
35. D. HULL, "Introduction to Dislocations" (Pergamon Press, London, 1968) p. 245.

Received 15 April
and accepted 13 August 2003